Chimeric constructs endow the human CFTR Cl^- channel with the gating behavior of murine CFTR

Toby S. Scott-Ward[†], Zhiwei Cai[†], Elizabeth S. Dawson[‡], Ann Doherty[‡], Ana Carina Da Paula[§], Heather Davidson[‡], David J. Porteous[‡], Brandon J. Wainwright[¶], Margarida D. Amaral[§‖], David N. Sheppard[†,††], and A. Christopher Boyd[‡]

[†]Department of Physiology and Pharmacology, University of Bristol, School of Medical Sciences, University Walk, Bristol BS8 1TD, United Kingdom; [‡]Medical Genetics Section, University of Edinburgh, Molecular Medicine Centre, Western General Hospital, Edinburgh EH4 2XU, United Kingdom; [¶]Institute for Molecular Bioscience, University of Queensland, Brisbane, Queensland 4072, Australia; [§]Centre of Human Genetics, National Institute of Health, Avenue Padre Cruz, 1649-016 Lisbon, Portugal; and [‖]Department of Chemistry and Biochemistry, Faculty of Sciences, University of Lisboa, Campo Grande-C8, 1749-016 Lisbon, Portugal

Edited by Michael J. Welsh, University of Iowa, Iowa City, IA, and approved August 16, 2007 (received for review February 20, 2007)

The cystic fibrosis transmembrane conductance regulator (CFTR) is a Cl^- channel gated by ATP-driven nucleotide-binding domain (NBD) dimerization. Here we exploit species differences between human and murine CFTR to investigate CFTR channel gating. Using homologous recombination, we constructed human-murine CFTR (hmCFTR) chimeras with sequences from NBD1, NBD2, or the regulatory domain (RD) of human CFTR replaced by the equivalent regions of murine CFTR. The gating behavior of hmRD and human CFTR were indistinguishable, whereas hmNBD1 and hmNBD2 had subtle effects on channel gating, prolonging both burst duration and interburst interval. By contrast, hmNBD1+2, containing both NBDs of murine CFTR, reproduced the gating behavior of the subconductance state of murine CFTR, which has dramatically prolonged channel openings. The CFTR potentiator pyrophosphate (PP_i) enhanced human, hmRD, and hmNBD1 CFTR Cl^- currents, but not those of hmNBD2, hmNBD1+2, and murine CFTR. By analyzing the rate-equilibrium free-energy relationships of chimeric channels, we obtained snapshots of the conformation of the NBDs during ATP-driven dimerization. Our data demonstrate that the conformation of NBD1 changes before that of NBD2 during channel opening. This finding suggests that NBD dimerization does not proceed by a symmetric tweezer-like motion, but instead in an asymmetric fashion led by NBD1. We conclude that the NBDs of murine CFTR determine the unique gating behavior of its subconductance state, whereas NBD2 controls channel potentiation by PP_i.

ATP-binding cassette transporter | chloride ion channel | cystic fibrosis | recombinational cloning | rate-equilibrium free-energy relationships

Mutation of the cystic fibrosis transmembrane conductance regulator (CFTR) Cl^- channel causes the genetic disease cystic fibrosis (CF) (1). CFTR is composed of two membrane-spanning domain (MSD)-nucleotide-binding domain (NBD) motifs linked by a unique regulatory domain (RD) (1). The MSDs assemble to form a low-conductance (6- to 10-pS) anion-selective pore (2). The RD contains multiple consensus phosphorylation sites, phosphorylation of which is a prerequisite for channel opening (2). The NBDs form a head-to-tail dimer with two ATP-binding sites located at the dimer interface (3). ATP binds tightly to one ATP-binding site (site 1; formed by the Walker A and B motifs of NBD1 and the LSGGQ motif of NBD2), whereas ATP is hydrolyzed rapidly at the other ATP-binding site (site 2; formed by the Walker A and B motifs of NBD2 and the LSGGQ motif of NBD1) (4, 5). Anion flow through the CFTR pore is gated by the interaction of ATP with sites 1 and 2 powering NBD dimerization and, hence, conformational changes in the MSDs (5).

A powerful strategy to investigate structure–function relationships is to exploit functional differences between homologues from divergent species. In previous work, we demonstrated that the gating behavior of murine CFTR (mCFTR) differs from that of human CFTR (hCFTR) in several important respects (6, 7). First, mCFTR opens for prolonged periods to a subconductance state (O_1) and only briefly transits to the full open state (O_2). Second, the open probability (P_o) of O_1 is greater than that of the full open state of hCFTR, whereas the P_o of O_2 is dramatically reduced. Third, AMP-PNP and pyrophosphate (PP_i), two agents that potentiate robustly hCFTR, do not affect mCFTR. Here, we exploit these species differences to investigate CFTR structure and function.

Because the NBDs and RD control CFTR channel gating (2), we reasoned that sequences within these domains most likely determine the differences in channel gating between hCFTR and mCFTR. To test this hypothesis, we constructed human-murine CFTR (hmCFTR) chimeras by replacing all or part of NBD1, the RD, or NBD2 with the equivalent regions of mCFTR, and we investigated their gating behavior using single-channel recording and kinetic analyses of channel gating. Moreover, by performing a rate-equilibrium free-energy relationships (REFER) analysis of hmCFTR chimeras, we probed the conformation of the NBDs during channel gating.

Results

Homologous Recombination Generates a Library of hmCFTR Chimeras. To construct hmCFTR chimeras, we used a recombination-based cloning strategy (Fig. 1*A*) (8). In this *in vivo* cloning method, the target domain of mCFTR is amplified by PCR using primers that contain hCFTR sequences at their 5′ ends, and the hCFTR cDNA is linearized within the domain of interest by restriction enzyme digestion before recombinogenic *E. coli* are cotransformed with the linearized hCFTR cDNA and the amplified mCFTR domain. The enzymatic machinery of the recombinogenic *E. coli* then promotes homologous recombination to produce a chimeric CFTR construct.

Based on the molecular model of NBD1 proposed by Annereau *et al.* (9) and consonant with subsequent studies (e.g., ref. 3), we revised the boundaries of the NBDs and RD used for *in vivo* cloning of chimeric cDNA constructs (Fig. 1*B*). Because of the high degree of homology between hCFTR and mCFTR sequences within the NBDs (identity at the amino acid level: NBD1, 81%; NBD2, 84%) (10), homologous recombination frequently occurred within these domains of mCFTR, rather than at the chimeric junctions defined by the PCR primers. As a result, we generated multiple different

Author contributions: T.S.S.-W. and Z.C. contributed equally as first authors; D.N.S. and A.C.B. contributed equally as senior authors, D.J.P., M.D.A., D.N.S., and A.C.B. designed research; T.S.S.-W., Z.C., E.S.D., A.D., A.C.D.P., and H.D. performed research; B.J.W. contributed new reagents/analytic tools; T.S.S.-W., Z.C., M.D.A., and A.C.B. analyzed data; and D.N.S. wrote the paper.

The authors declare no conflict of interest.

This article is a PNAS Direct Submission.

Abbreviations: CF, cystic fibrosis; CFTR, cystic fibrosis transmembrane conductance regulator; MSD, membrane-spanning domain; NBD, nucleotide-binding domain; O_1, subconductance state of murine CFTR; O_2, full open state of murine CFTR; P_o, open probability; PP_i, pyrophosphate; RD, regulatory domain; REFER, rate-equilibrium free-energy relationships.

[††]To whom correspondence should be addressed. E-mail: D.N.Sheppard@bristol.ac.uk.

This article contains supporting information online at www.pnas.org/cgi/content/full/0701562104/DC1.

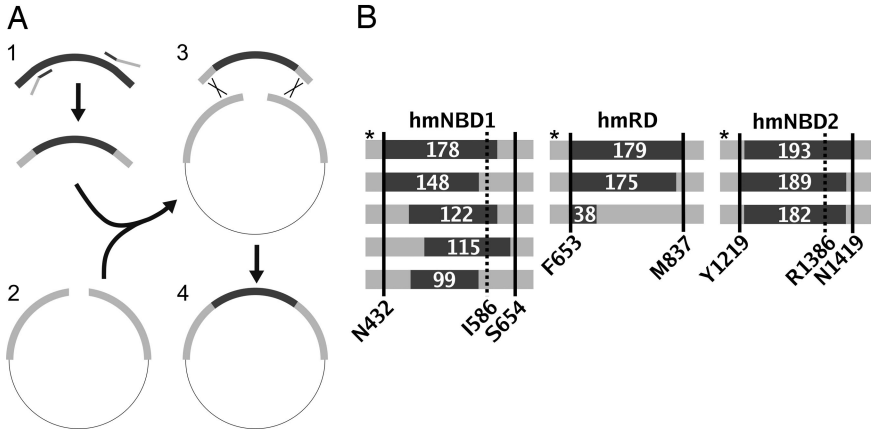

Fig. 1. Generation of hmCFTR chimeras. (*A*) Scheme for chimera generation. Dark- and light-gray segments denote mCFTR and hCFTR, respectively, whereas homologous recombination is indicated by cross-over lines. (*B*) Schematic diagrams of hmCFTR chimeras. The dark-gray segments represent mCFTR (numbers, length in mCFTR amino acid residues), and the light-gray rectangles represent hCFTR. The continuous lines and coordinates indicate domain boundaries, whereas the dashed lines and coordinates show the original C termini of NBD1 and NBD2 (1). Asterisks identify the chimeras selected for study. For further information, see *Materials and Methods* and *SI Text*.

cDNA constructs during the cloning of hmNBD1 and hmNBD2 [Fig. 1*B* and supporting information (SI) Table 1]. For hmNBD2 one construct had a genotype equivalent to 97% of the primer design, whereas for hmNBD1 the highest degree of identity was 80% (SI Table 1). Despite reduced sequence homology between the RDs of hCFTR and mCFTR (69% identity) (10), we generated three different constructs during the cloning of hmRD, one of which had a genotype identical to that of the primer design (SI Table 1). Thus, by using an *in vivo* cloning strategy, we generated a series of hmCFTR chimeras possessing different amounts of mCFTR sequence on an hCFTR background.

For biochemical and functional studies, we selected the CFTR chimeras containing the largest amount of mCFTR sequence [hmNBD1–562c, hmRD-96a (or hmRD-64a) (SI Table 1), and hmNBD2–323c containing 178, 179, and 193 contiguous residues of mCFTR, respectively, which we, hereafter term hmNBD1, hmRD, and hmNBD2]. Because the NBDs of ATP-binding cassette transporters function as a head-to-tail dimer (11), we also studied a CFTR chimera containing both mCFTR NBDs (hmNBD1+2), which we constructed from hmNBD1 and hmNBD2 by conventional cloning techniques.

hmCFTR Chimeras Generate the Mature Form of CFTR Protein. CFTR exists in two different forms: an immature core-glycosylated form found in the ER (150 kDa, band B) and a mature, fully glycosylated form that is processed by the Golgi apparatus (170–180 kDa, band C). To determine whether hmCFTR chimeras exit the ER, we monitored their processing by Western blotting. SI Fig. 5 shows that a specific anti-CFTR antibody detected both the immature and mature forms of CFTR in HEK293 cells transiently expressing wild-type and chimeric CFTRs. These data demonstrate that hmCFTR chimeras are fully processed to post-Golgi compartments.

Transfer of the Gating Behavior of mCFTR to hCFTR. To investigate the gating behavior of chimeric CFTR Cl^- channels, we transiently expressed CFTR constructs in CHO cells and studied single Cl^- channels in excised inside-out membrane patches. Fig. 2 shows representative single-channel recordings of wild-type and chimeric CFTR Cl^- channels after phosphorylation by PKA. Several important points are apparent from visual inspection of these records. First, the single-channel current amplitude of hmCFTR chimeras is similar to that of hCFTR and much larger than that of mCFTR (Fig. 2). Moreover, hCFTR and hmCFTR chimeras open predominantly to the full open state; transitions to subconductance states are unusual for these channels (Fig. 2). In contrast, mCFTR resides infrequently in the full open state (O_2) (Fig. 2). Instead, it dwells principally in a tiny subconductance state (O_1), which is resolved by filtering heavily single-channel records (Fig. 2). To quantify Cl^- flow, we measured single-channel conductance (SI Fig. 6). All hmCFTR chimeras had single-channel conductances similar to that of hCFTR and larger than the O_1 and O_2 states of mCFTR (SI Fig. 6). These data argue that the architecture of the channel pore in hmCFTR chimeras is similar to that of hCFTR.

Second, the patterns of gating of hmCFTR chimeras are intermediate between those of hCFTR and mCFTR. The gating behavior of hCFTR is characterized by short bursts of channel openings interrupted by brief flickery closures and separated by longer

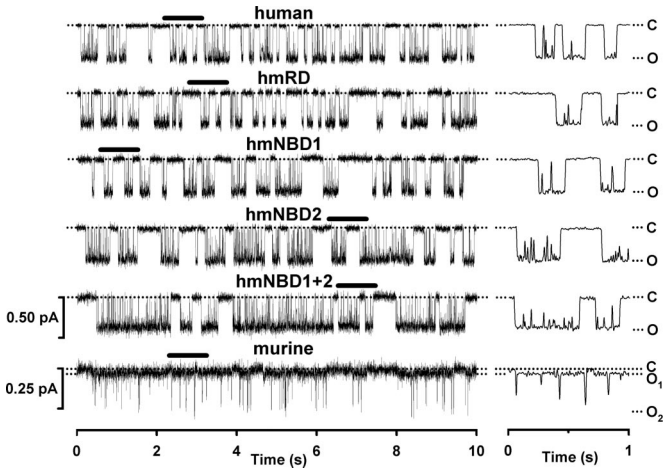

Fig. 2. The single-channel activity of wild-type and chimeric CFTRs. Representative single-channel recordings of wild-type and chimeric CFTRs in excised inside-out membrane patches from CHO cells expressing the indicated CFTR variants. In this and subsequent figures, unless otherwise indicated, 0.3 mM ATP and 75 nM PKA were continuously present in the intracellular solution, voltage was −50 mV, and there was a large Cl^- concentration gradient across the membrane ($[Cl^-]_{int}$, 147 mM; $[Cl^-]_{ext}$, 10 mM). The closed-channel state (C), the subconductance state of mCFTR (O_1), and the full open state (hCFTR and hmCFTR chimeras, O; mCFTR, O_2) are indicated by dotted lines. Traces on the left were filtered at 500 Hz, whereas the 1-s portions indicated by bars shown on an expanded time scale to the right were filtered at 50 Hz.

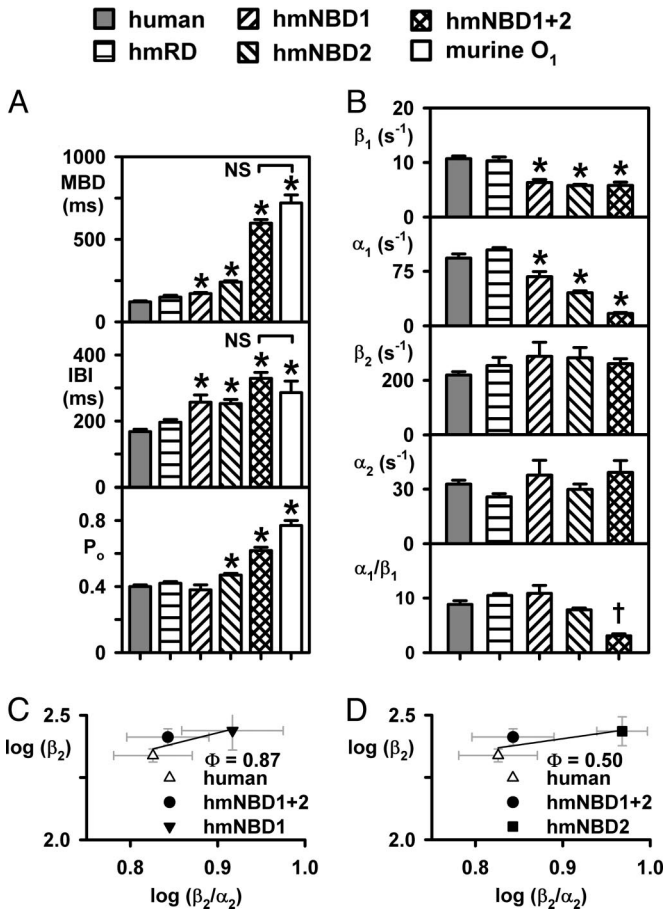

Fig. 3. Chimeric CFTRs alter entry to and exit from the bursting state. (*A*) Mean burst duration (MBD), interburst interval (IBI), and open probability (P_o) of the indicated CFTR variants. (*B*) Rate and equilibrium dissociation (α_1/β_1) constants for wild-type and chimeric CFTRs determined by the maximum likelihood fit to the model shown in Scheme 1. Because mCFTR possesses two open states and three closed states, Scheme 1 is unsuitable for modeling its gating behavior. In *A* and *B*, data are means + SEM ($n = 5$; except hmNBD1, $n = 4$; hmRD, $n = 3$). Asterisks indicate values that are significantly different from those of hCFTR ($P < 0.05$), and the cross indicates a value that is significantly different from those of other CFTR constructs (one-way ANOVA, $P < 0.001$). NS, not significant. (*C* and *D*) Brønsted plots for hmNBD1 and hmNBD2, respectively, determined by using the data shown in *B*. The continuous lines are the fits of first-order regressions to the data. For further information, see *Results* and *SI Text*.

closures between bursts (Fig. 2). In contrast, mCFTR resides for prolonged periods in O_1, from which it makes short-lived sojourns to O_2 and longer visits to closed periods between bursts (Fig. 2). The pattern of hmRD gating closely resembles that of hCFTR, whereas the gating of hmNBD1 and hmNBD2 shows subtle differences from that of hCFTR (Fig. 2). For hmNBD1 and hmNBD2, both the duration of channel openings and the closed-time interval between bursts are prolonged compared with those of hCFTR (Fig. 2). However, these chimeric channels still open for much shorter periods than the O_1 state of mCFTR. Strikingly, the burst duration of hmNBD1+2 is prolonged markedly compared with that of hCFTR, while its closed-time interval between bursts is also extended (Fig. 2).

To quantify gating behavior, we analyzed the distribution of dwell times by using membrane patches that contained only a single active channel (see SI Fig. 7 and SI Table 2) and performed an analysis of bursts (Fig. 3*A*). Several conclusions can be drawn from these analyses. First, the burst duration, interburst interval, and P_o of hCFTR and hmRD were equivalent (Fig. 3*A*). Second, for hmNBD1 and hmNBD2, both burst duration and interburst interval were prolonged compared with those of hCFTR. In consequence, the P_o of hmNBD1 did not differ from that of hCFTR, whereas that of hmNBD2 was slightly increased ($P = 0.005$) (Fig. 3*A*). Third, the burst duration of hmNBD1+2 was prolonged 392% compared with that of hCFTR, whereas the interburst interval was lengthened 96% (Fig. 3*A*). As a result, the P_o of hmNBD1+2 was 54% greater than that of hCFTR (Fig. 3*A*). Fourth, although the P_o of hmNBD1+2 was less than that of the O_1 state of mCFTR ($P = 0.007$), values of burst duration and interburst interval for hmNBD1+2 and the O_1 state of mCFTR were statistically indistinguishable (Fig. 3*A*). These data suggest that transfer of both NBDs of mCFTR endows hCFTR with the gating behavior of the O_1 state of mCFTR.

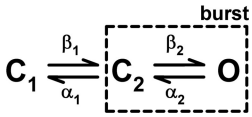

Scheme 1. A linear three-state model of CFTR channel gating (12). States enclosed within the dashed box represent the bursting state. For further information, see *Results*.

To calculate the transition rates for entry to and exit from bursts of channel openings, we used maximum likelihood analysis and kinetic modeling. Scheme 1 shows the simplest model to describe CFTR channel gating (12). In Scheme 1, C_1 represents the long-duration, closed state separating channel openings, and $C_2 \leftrightarrow O$ represents the bursting state in which channel openings (O) are interrupted by brief flickery closures (C_2). Transitions between the three states are described by the rate constants β_1, β_2, α_1, and α_2.

Fig. 3*B* summarizes the rate constants of Scheme 1 for hmCFTR chimeras. The rate constants of hmRD were indistinguishable from those of hCFTR. In contrast, those of hmNBD1, hmNBD2, and hmNBD1+2 differed markedly. For each construct, β_1 was decreased by ≈40%; α_1 was decreased by 27%, 51%, and 82% for hmNBD1, hmNBD2, and hmNBD1+2, respectively; and β_2 and α_2 were unaltered (Fig. 3*B*). The decrease in β_1 lengthens the interburst interval by slowing entry into the bursting state. Conversely, the decrease in α_1 increases burst duration by delaying exit from the bursting state. Thus, transfer of mCFTR NBDs to hCFTR slows channel gating by decreasing the frequency of channel openings and prolonging their duration.

The NBDs of mCFTR Enhance the ATP Sensitivity of hCFTR. CFTR channel gating is tightly controlled by the interaction of ATP with two binding sites located at the interface of the NBD dimer (3, 5). Therefore, we speculated that differences in gating behavior between hCFTR and hmCFTR chimeras might reflect altered affinities and/or efficacies of chimeric channels for ATP. To test this hypothesis, we examined the ATP dependence of channel gating using membrane patches containing small numbers of active channels.

Fig. 4*A* demonstrates that as the ATP concentration increased, the activity of both hCFTR and hmCFTR chimeras increased. However, hmCFTR chimeras exhibited enhanced ATP sensitivity and channel activity compared with hCFTR. These differences are best illustrated by considering values of K_D (the ATP concentration required for half maximal activity, which describes the apparent affinity of CFTR for ATP) and $P_{o\ max}$ (the maximum P_o) determined from Michaelis–Menten fits to the mean data (hCFTR: $K_D = 167\ \mu M$, $P_{o\ max} = 0.57$, $r^2 = 0.98$; hmNBD1: $K_D = 100\ \mu M$, $P_{o\ max} = 0.55$, $r^2 = 0.99$; hmNBD2: $K_D = 109\ \mu M$, $P_{o\ max} = 0.68$, $r^2 = 0.99$; hmNBD1+2: $K_D = 63\ \mu M$, $P_{o\ max} = 0.74$, $r^2 = 0.99$). Several conclusions are apparent from these data. First, mCFTR NBD2, but not mCFTR NBD1, augments channel activity. Second, NBD1 and NBD2 of mCFTR each enhance the apparent ATP affinity of chimeric channels. Third, the apparent ATP affinity of

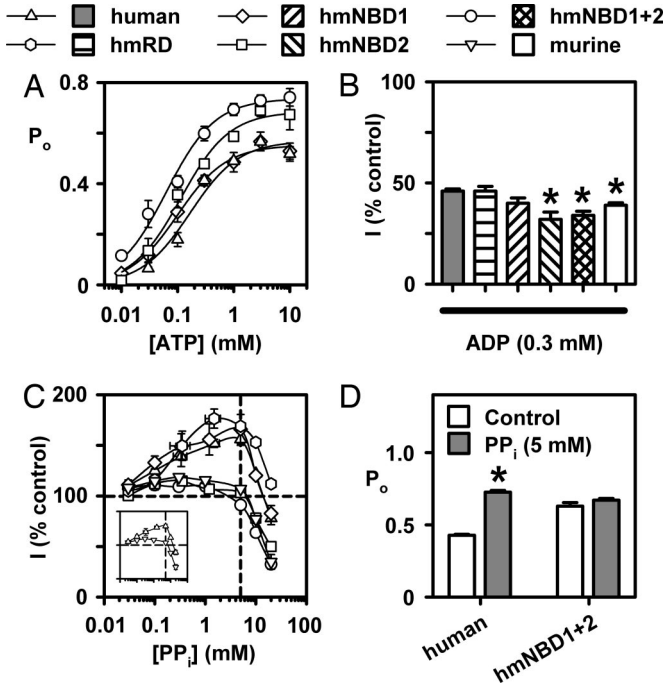

Fig. 4. The nucleotide dependence of wild-type and chimeric CFTRs. (*A*) The relationship between ATP concentration and P_o for the indicated chimeric CFTRs. The continuous lines are Michaelis–Menten fits to the mean data. (*B*) ADP inhibition of CFTR constructs. CFTR Cl^- currents measured in the presence of 0.3 mM ADP are expressed as a percentage of control currents. (*C*) The relationship between PP_i concentration and CFTR Cl^- current for wild-type and chimeric CFTRs. CFTR Cl^- currents measured in the presence of 0.03–20 mM PP_i are expressed as a percentage of control currents. Values above and below the horizontal dashed line indicate CFTR potentiation and inhibition, respectively. (*Inset*) Data for hCFTR and mCFTR alone. (*D*) Effects of 1 mM PP_i on the P_o of hCFTR and hmNBD1+2. All data are means + SEM (n = 4–5; except in *C*, where the data for hmRD are n = 1–5). In *B* and *D*, the asterisks indicate values that are significantly different from hCFTR and control values, respectively ($P < 0.05$).

hmNBD1+2 suggests that the effects of mCFTR NBD1 and NBD2 on the apparent ATP affinity of chimeric channels are additive.

To gain deeper insight into the ATP affinity of CFTR chimeras and the efficacy with which ATP gates them, we investigated further the kinetics of channel gating. Given that CFTR is an agonist-activated channel gated by intracellular ATP (2, 4) and Scheme 1 is reminiscent of the classical del Castillo–Katz mechanism (Scheme 2) (13, 14), we can calculate the ATP affinity and efficacy of CFTR constructs. In Scheme 2, R represents the closed channel, R* represents the open channel, and A represents the agonist (ATP for CFTR). The agonist equilibrium dissociation constants (K_A: Scheme 2, K_{-1}/K_{+1}; Scheme 1, α_1/β_1) reflects agonist binding to the channel (i.e., ATP affinity), whereas the equilibrium constant between the closed and open states of the channel (*E:* Scheme 2, β/α; Scheme 1, β_2/α_2) reflects channel gating (i.e., ATP efficacy) (14).

Fig. 3*B* compares the equilibrium dissociation constants of

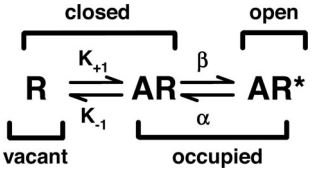

Scheme 2. The del Castillo–Katz mechanism. For further information, see *Results*.

wild-type and chimeric CFTRs. For hmRD, hmNBD1, and hmNBD2, α_1/β_1 values did not differ from that of hCFTR, whereas the α_1/β_1 value of hmNBD1+2 was 65% smaller than that of hCFTR ($P < 0.001$) (Fig. 3*B*), which is in excellent agreement with the difference in K_D values (62%) (Fig. 4*A*). These data suggest that only hmNBD1+2 has a greater ATP affinity than hCFTR. However, all of the CFTR chimeras had β_2/α_2 values similar to that of hCFTR (one-way ANOVA, $P > 0.05$; n = 3–5; data not shown), suggesting that ATP gates hCFTR and hmCFTR chimeras with equal efficacy.

To investigate how ATP binding by the NBDs drives conformation changes in CFTR during channel gating, we performed a REFER analysis (see *SI Text*) (15, 16). Using this approach, Auerbach and colleagues (15, 16) mapped the conformational changes in the nicotinic acetylcholine receptor that accompany channel opening. We were particularly interested to learn whether a REFER analysis of hmCFTR chimeras might provide spatial and temporal information about the NBDs during ATP-driven channel gating. Toward this aim, we used the transition rates β_2 and α_2 to generate Brønsted plots [log (β_2) plotted vs. log (β_2/α_2)] of hmNBD1 and hmNBD2 (Fig. 3 *C* and *D* and SI Fig. 8). The slope of the line in a Brønsted plot (Φ) quantifies the relative extent to which the opening (β_2) and closing (α_2) rate constants change, and it also provides an estimate of the temporal sequence of intermediate events during channel gating. Values of Φ range between 0 and 1. When Φ is close to 1, the transition state resembles an open-channel conformation and moves early during gating, whereas when Φ is close to 0, the transition state resembles a closed-channel conformation and moves late during gating (15, 16). For hmNBD1, Φ = 0.87 (r^2 = 0.67), and for hmNBD2, Φ = 0.50 (r^2 = 0.58) (Fig. 3 *C* and *D*). These data argue that, during the transition state, NBD1 adopts a conformation resembling an open channel, whereas that of NBD2 is intermediate between the open and closed states. These findings suggest that, during channel opening, NBD1 moves before NBD2.

ADP Inhibits Wild-Type and Chimeric CFTRs. ADP, one product of ATP hydrolysis, inhibits hCFTR and mCFTR (6). Fig. 4*B* shows that ADP reduced markedly the activity of hmCFTR chimeras. The ADP sensitivities of hCFTR, hmRD, and hmNBD1 were equivalent (Fig. 4*B*). However, ADP inhibited hmNBD2, hmNBD1+2, and mCFTR more potently than hCFTR (Fig. 4*B*), suggesting that the ADP sensitivity of mCFTR exceeds that of hCFTR.

NBD2 Determines the PP_i Sensitivity of hCFTR. The CFTR potentiator PP_i interacts directly with the NBDs of hCFTR to potentiate robustly CFTR channel gating (17). However, PP_i does not affect mCFTR (6). To identify the protein regions responsible for this species difference, we investigated the effects of PP_i on hmCFTR chimeras.

Fig. 4*C* summarizes the PP_i concentration–response relationships of wild-type and chimeric CFTRs. Inspection of the data reveals two types of concentration–response relationships. For hCFTR, hmNBD1, and hmRD, current magnitude enlarged progressively as the PP_i concentration increased in the micro- and low millimolar range, reaching a peak at ≈70% above the control value (Fig. 4*C*). For hCFTR and hmNBD1 the maximal current occurred at 5 mM PP_i, whereas for hmRD it occurred at 1 mM PP_i. By increasing further the PP_i concentration, the current magnitude declined markedly.

For mCFTR, hmNBD2, and hmNBD1+2, there was little or no current potentiation at low PP_i concentrations (Fig. 4*C*). The maximal current achieved was only ≈20% above the control value and occurred at 0.3 mM PP_i. However, when the PP_i concentration exceeded 5 mM, current magnitude decayed sharply. Taken together, the data suggest that PP_i interacts with sequences in NBD2 to potentiate CFTR, but sequences in both NBDs to inhibit CFTR.

To understand better why PP_i potentiated CFTR constructs

containing hCFTR NBD2, but not those containing mCFTR NBD2, we studied single Cl^- channels. Fig. 4*D* demonstrates that 1 mM PP_i enhanced the P_o of hCFTR, but not that of hmNBD1+2. These data suggest that the activity of individual CFTR Cl^- channels determines their response to PP_i. Channels with modest P_o values are potentiated by PP_i, whereas those with high P_o values are insensitive to PP_i. Thus, the behavior of chimeric CFTR Cl^- channels is a consequence of their acquisition of unusual properties from mCFTR.

Discussion

In this study, we exploited species differences to investigate CFTR channel gating. We constructed hmCFTR chimeras by homologous recombination and investigated their behavior with single-channel recording and kinetic analyses of channel gating. By transfer of both NBDs of mCFTR to hCFTR, we endowed the human CFTR Cl^- channel with the gating behavior of the O_1 state of mCFTR, which has dramatically prolonged channel openings. However, transfer of mCFTR NBD2 alone sufficed to make the hCFTR Cl^- channel insensitive to potentiation by PP_i. Of note, by applying REFER analysis to hmCFTR chimeras, we obtained snapshots of the conformation of the NBDs during ATP-driven dimerization.

Molecular Mechanisms of ATP-Dependent Gating. Previous work has revealed asymmetries in the structure and function of CFTR's two NBDs (2, 4), suggesting that they might make different contributions to CFTR channel gating. Using chimeric proteins, we evaluated the contribution of individual NBDs to CFTR function. Transfer of either NBD1 or NBD2 of mCFTR had subtle effects on channel gating. Only by transferring both NBDs of mCFTR did we endow the hCFTR Cl^- channel with the prolonged channel openings of the O_1 state of mCFTR. Consistent with these results, both NBDs of CFTR are required for optimal ATPase activity (18). We interpret these results to suggest that the two NBDs of CFTR each make a critical contribution to CFTR channel gating.

Crystal structures of ATP-binding cassette transporters (e.g., BtuCD) (11) reveal that the NBDs associate to form a functional unit, the NBD dimer, which clamps two ATP molecules within binding sites located at the dimer interface. To investigate the dimerization of CFTR's NBDs, Vergani *et al.* (5) applied mutant cycle analysis to residues predicted to lie on opposite sides of the NBD dimer. Because R555 (NBD1) and T1246 (NBD2) were energetically coupled in open, but not closed, channels, the authors proposed that the NBDs undergo dynamic reorganization during channel gating, with the two NBDs associating tightly during channel opening (5). Our own data support the idea that optimal channel gating requires precise interactions between the two NBDs. However, the data also suggest that channel gating, albeit suboptimal, is possible when NBDs from two homologues are mixed. This finding raises the interesting possibility of using chimeric channels to investigate the gating cycle of NBDs from other ATP-binding cassette transporters.

Transfer of both NBDs of mCFTR to hCFTR slowed channel gating by decreasing the frequency of channel openings and prolonging markedly their duration. Using the ATP-driven NBD dimerization model of CFTR channel gating (5), we suggest that the energy barrier for dimerization of mCFTR NBDs is greater than that of hCFTR. However, once the mCFTR NBD dimer has formed, it has greater stability than that of hCFTR. Increased stability of the mCFTR NBD dimer might result from tighter ATP binding at site 2. Consistent with this idea, the ATP affinity of hmNBD1+2, which reflects binding at site 2 (5), greatly exceeded that of hCFTR. Alternatively, or in addition, mCFTR site 2 might hydrolyze ATP more slowly than hCFTR.

One prediction of the ATP-driven NBD dimerization model (5) is that dynamic reorganization of the NBD dimer drives conformation changes leading to Cl^- flow through the pore. This prediction suggests that there might be one (or more) transient intermediate stages of the conformational change between ATP binding and channel opening. CFTR might change its conformation synchronously. Alternatively, there might be a wave of conformational change that sweeps across the protein. In support of the latter idea, using REFER analysis, Auerbach and colleagues (15, 16) demonstrated that ligand binding to the acetylcholine receptor initiates a wave of conformational change that begins at the ligand-binding site and propagates through the transmembrane segments, which move in three discrete steps, to the site of voltage regulation. Our present data preclude a systematic analysis of the conformational changes in CFTR that follow ATP binding. However, by performing REFER analyses on the NBD chimeras and wild-type CFTR gated by ATP and membrane voltage (see SI Fig. 8), we obtained snapshots of the conformations of the NBDs and MSDs at the transition state. Our data indicate that the NBDs move before the MSDs during channel opening. This result suggests that a wave of conformational change propagates from the NBDs to the MSDs. The data also reveal that NBD1 adopts a conformation resembling an open channel, whereas that of NBD2 is intermediate between the open and closed states. These findings argue that, during the transition state, the conformation of NBD1 changes before that of NBD2. Thus, NBD dimerization does not proceed by a symmetric tweezer-like motion, but instead in an asymmetric fashion led by NBD1.

Site of Action of CFTR Potentiators. Some CFTR potentiators enhance CFTR channel gating by binding at the interface of the NBD dimer (19–21). However, our data demonstrate that NBD2 alone determines whether PP_i potentiates CFTR activity. This finding argues that sequences in NBD2 form the PP_i-binding site.

If sequences in NBD2 form the PP_i-binding site, where might they be located? Randak and Welsh (22) demonstrated that CFTR has adenylate kinase activity that regulates channel gating. This enzymatic activity is localized to NBD2, which possesses distinct ATP- and AMP-binding sites. Perhaps differences between the AMP-binding sites of hCFTR and mCFTR might account for their altered sensitivities to PP_i. Because ADP inhibits CFTR, in part, through the adenylate kinase activity of NBD2 (23), the different sensitivities of hCFTR and mCFTR to ADP also might reflect differences at the AMP-binding site. Support for these ideas is provided by the CF mutant N1303K, which attenuates greatly CFTR potentiation by PP_i, inhibition by ADP, and adenylate kinase-dependent channel gating (22, 24). Although N1303 is conserved in mCFTR, this region of NBD2 contains a cluster of sequence changes between hCFTR and mCFTR (SI Fig. 9). Future studies should test whether these differences account for the altered sensitivity of mCFTR to PP_i.

Elevated concentrations of some CFTR potentiators inhibit the CFTR Cl^- channel. This inhibition is principally caused by a dramatic slowing of channel opening (allosteric block), but also may involve pore occlusion (open-channel block) (25). Because elevated concentrations of PP_i inhibited all CFTR constructs and prolonged markedly the interburst interval of hCFTR (present results and data not shown), we conclude that allosteric block by PP_i involves sequences from both NBDs. For several reasons, we speculate that allosteric blockers might interact with site 2 to impede NBD dimerization. First, CFTR inhibition by allosteric blockers is relieved by high concentrations of ATP (e.g., genistein) (25). Second, many CFTR potentiators, by themselves, do not support channel activity (e.g., PP_i) (17), arguing that they do not interact at site 1. Third, allosteric block of CFTR by genistein is abolished by mutation of G551 in site 2 (26). Thus, PP_i might potentiate CFTR by interacting with the AMP-binding site and inhibit CFTR by binding at site 2.

Implications for Therapy. Mouse models of CF have been widely used to evaluate new therapies for CF. For example, gentamicin improves the survival of G542X CF mice (27) and rescues CFTR

function in CF patients bearing stop codon mutations (28). By contrast, curcumin rescued the ion transport defect of F508del CF mice (29), but not CF patients homozygous for the F508del mutation.[‡‡] Based on the present results, functional differences between hCFTR and mCFTR might, in part, account for the failure of some therapies identified in CF mice to be efficacious in CF patients.

Materials and Methods

Construction of hmCFTR Chimeras. We adapted a homologous recombination-based system for gene therapy vector construction to generate plasmids of hmCFTR chimeras (Fig. 1*A*). In brief, (*i*) the target domain of mCFTR cDNA in the plasmid pFLM-CFTR was amplified by PCR using primers that contain hCFTR sequence at their 5′ ends; (*ii*) the plasmid pCMV-CFTR containing the hCFTR cDNA was linearized in the domain of interest; (*iii*) the products of *i* and *ii* were coelectroporated into the recombinogenic *E. coli* strain DH10B-U/pSpRecGam (8); and (*iv*) intact chimeric plasmids were recovered when intermolecular recombination occurred between homologous sequences of linear pCMV-CFTR and the PCR products. All constructs were sequenced exhaustively before biochemical and functional analyses. We defined the extent of mCFTR sequence in each chimera not by the points at which DNA recombination occurred (which are not always determinable), but instead by the largest contiguous block of deduced protein sequence that exactly matches the corresponding mCFTR sequence. For example, in hmNBD1, the 3′ DNA recombination site is near I586. However, because of perfect protein sequence homology downstream of this residue, we report the amount of mCFTR NBD1 attributed to hmNBD1 as extending to L610 (SI Fig. 9). Intradomain boundaries of chimeras, where specified, are given as the hCFTR amino acid residues flanking the contiguous mCFTR sequence tracts (for more details, see *SI Text*).

Cells and CFTR Expression. We transiently expressed CFTR variants with GFP in CHO cells by using Lipofectamine Plus (Invitrogen, Carlsbad, CA). Then 36–60 h after transfection, we selected GFP expressing cells for study.

Electrophysiology. CFTR Cl^- channels were recorded in excised inside-out membrane patches by using an Axopatch 200B patch-clamp amplifier and pCLAMP software (both from Molecular Devices, Sunnyvale, CA) as described (25). The pipette (extracellular) solution contained 140 mM NMDG, 140 mM aspartic acid, 5 mM $CaCl_2$, 2 mM $MgSO_4$, and 10 mM TES (pH 7.3 with Tris) ([Cl^-], 10 mM). The bath (intracellular) solution contained 140 mM NMDG, 3 mM $MgCl_2$, 1 mM CsEGTA, and 10 mM TES (pH 7.3 with HCl) ([Cl^-], 147 mM; free $Ca^{2+} < 10^{-8}$ M) and was maintained at 37°C; voltage was −50 mV.

To investigate the effects of PP_i and ADP, we used membrane patches containing multiple active channels. For all other studies, membrane patches contained less than or equal to four active channels. The number of channels in a membrane patch was determined from the maximum number of simultaneous channel openings observed during a recording (21).

We recorded, filtered, and digitized data as described (25), with the exception that single-channel records of mCFTR were subsequently digitally filtered at 50 Hz before analysis. For the purpose of illustration, single-channel records were filtered at either 50 or 500 Hz and digitized at 1 kHz. P_o was calculated, and burst analysis was performed as described (21).

Modeling of Single-Channel Kinetics and REFER Analysis. To perform maximum likelihood analysis and develop kinetic models of channel gating, we used QuB software (www.qub.buffalo.edu) (21). To investigate conformational changes during channel gating, we performed a REFER analysis (*SI Text*) (15, 16). For two reasons, this approach is feasible with hmCFTR chimeras. First, the difference in Gibb's free energy between hCFTR and hmCFTR chimeras is small (SI Table 4). Second, hmCFTR chimeras have the same conductance and regulation as hCFTR. Thus, hmCFTR chimeras do not perturb the global structure of CFTR. Only membrane patches that contained a single active channel were used for maximum likelihood analysis, kinetic modeling, and REFER analysis.

Reagents. With the exception of PKA (Promega, Southampton, U.K.), chemicals were purchased from Sigma–Aldrich (Gillingham, U.K.). Stock solutions of PP_i were prepared as described (17), whereas those for ATP and ADP were prepared immediately before use. We increased the Mg^{2+} concentration of the intracellular solution to 10 mM when studying the ATP dependence of hmCFTR chimeras at ATP concentrations ≥3 mM. To maintain a constant MgATP concentration in intracellular solutions containing different PP_i concentrations, we added varying Na_2ATP concentrations calculated by using Bound and Determined software (30).

Statistics. Results are expressed as means ± SEM of *n* observations. To compare sets of data, we used either an ANOVA or Student's *t* test. Differences were considered statistically significant when $P < 0.05$.

We thank A. A. Aleksandrov, C. E. Bear, O. Moran, P. J. Thomas, and our departmental colleagues for valuable discussions and Z. Xu and L. S. Pissarra for excellent assistance. This work was supported by the Biotechnology and Biological Sciences Research Council, Cystic Fibrosis Trust, Fundação para a Ciência a Tecnlogia Grant POCTI/MGI/47382/2002, and the Medical Research Council.

[‡‡]Egan, M., 27th European Cystic Fibrosis Conference, June 13–17, 2004, Birmingham, U.K.

1. Riordan JR, Rommens JM, Kerem B-S, Alon N, Rozmahel R, Grzelczak Z, Zielenski J, Lok S, Plavsic N, Chou J-L, *et al.* (1989) *Science* 245:1066–1073.
2. Sheppard DN, Welsh MJ (1999) *Physiol Rev* 79:S23–S45.
3. Lewis HA, Buchanan SG, Burley SK, Conners K, Dickey M, Dorwart M, Fowler R, Gao X, Guggino WB, Hendrickson WA, *et al.* (2004) *EMBO J* 23:282–293.
4. Riordan JR (2005) *Annu Rev Physiol* 67:701–718.
5. Vergani P, Lockless SW, Nairn AC, Gadsby DC (2005) *Nature* 433:876–880.
6. Lansdell KA, Delaney SJ, Lunn DP, Thomson SA, Sheppard DN, Wainwright BJ (1998) *J Physiol* 508:379–392.
7. Lansdell KA, Kidd JF, Delaney SJ, Wainwright BJ, Sheppard DN (1998) *J Physiol* 512:751–764.
8. Walker WE, Porteous DJ, Boyd AC (2004) *J Control Release* 94:245–252.
9. Annereau J-P, Wulbrand U, Vankeerberghen A, Cuppens H, Bontems F, Tümmler B, Cassiman J-J, Stoven V (1997) *FEBS Lett* 407:303–308.
10. Tata F, Stanier P, Wicking C, Halford S, Kruyer H, Lench NJ, Scambler PJ, Hansen C, Braman JC, Williamson R, *et al.* (1991) *Genomics* 10:301–307.
11. Locher KP, Lee AT, Rees DC (2002) *Science* 296:1091–1098.
12. Winter MC, Sheppard DN, Carson MR, Welsh MJ (1994) *Biophys J* 66:1398–1403.
13. del Castillo J, Katz B (1957) *Proc R Soc Lond B Biol Sci* 146:369–381.
14. Colquhoun D (1998) *Br J Pharmacol* 125:923–947.
15. Grosman C, Zhou M, Auerbach A (2000) *Nature* 403:773–776.
16. Purohit P, Mitra A, Auerbach A (2007) *Nature* 446:930–933.
17. Carson MR, Winter MC, Travis SM, Welsh MJ (1995) *J Biol Chem* 270:20466–20472.
18. Kidd JF, Ramjeesingh M, Stratford F, Huan L-J, Bear CE (2004) *J Biol Chem* 279:41664–41669.
19. Ai T, Bompadre SG, Wang X, Hu S, Li M, Hwang T-C (2004) *Mol Pharmacol* 65:1415–1426.
20. Moran O, Galietta LJV, Zegarra-Moran O (2005) *Cell Mol Life Sci* 62:446–460.
21. Cai Z, Taddei A, Sheppard DN (2006) *J Biol Chem* 281:1970–1977.
22. Randak C, Welsh MJ (2003) *Cell* 115:837–850.
23. Randak CO, Welsh MJ (2005) *Proc Natl Acad Sci USA* 102:2216–2220.
24. Berger AL, Ikuma M, Hunt JF, Thomas PJ, Welsh MJ (2002) *J Biol Chem* 277:2125–2131.
25. Lansdell KA, Cai Z, Kidd JF, Sheppard DN (2000) *J Physiol* 524:317–330.
26. Dérand R, Bulteau-Pignoux L, Becq F (2002) *J Biol Chem* 277:35999–36004.
27. Du M, Jones JD, Lanier J, Keeling KM, Lindsey JR, Tousson A, Bebok Z, Whitsett JA, Dey CR, Colledge WH, *et al.* (2002) *J Mol Med* 80:595–604.
28. Wilschanski M, Yahav Y, Yaacov Y, Blau H, Bentur L, Rivlin J, Aviram M, Bdolah-Abram T, Bebok Z, Shushi L, *et al.* (2003) *N Engl J Med* 349:1433–1441.
29. Egan ME, Pearson M, Weiner SA, Rajendran V, Rubin D, Glockner-Pagel J, Canny S, Du K, Lukacs GL, Caplan MJ (2004) *Science* 304:600–602.
30. Brooks SPJ, Storey KB (1992) *Anal Biochem* 201:119–126.